Available online at www.sciencedirect.com
SCIENCE DIRECT®
International Journal of Heat and Fluid Flow 26 (2005) 173–190
International Journal of HEAT AND FLUID FLOW
www.elsevier.com/locate/ijhff

A hybrid two-layer URANS–LES approach for large eddy simulation at high Reynolds numbers

L. Temmerman [a], M. Hadžiabdić [b], M.A. Leschziner [a,*], K. Hanjalić [b]

[a] Department of Aeronautics, Imperial College London, Prince Consort Road, London SW7 2BY, United Kingdom
[b] Thermofluids section, Faculty of Applied Sciences, Delft University of Technology, Lorentzweg 1, 2628 CJ Delft, The Netherlands

Received 22 January 2004; accepted 29 July 2004

Abstract

A hybrid RANS–LES methodology is proposed for simulating flows that demand a high-quality resolution of the near-wall region. The method allows the thickness of the near-wall RANS Layer to be chosen freely. This layer is interfaced to the outer LES region subject to compatibility conditions for velocity and turbulent viscosity imposed across the interface. These conditions are extracted dynamically as the simulation progresses. In the RANS layer, one-equation (k–l) and two-equations (k–ϵ) models are used and interfaced to the dynamic Smagorinsky or one-equation subgrid-scale models. The effectiveness of the method is assessed by reference to fully-developed channel flow at $Re_b = 10{,}935$ and $Re_b = 42{,}200$, and a separated flow at $Re_b = 21{,}560$ in a channel constricted by curved hill-shaped obstructions, for which both pure LES and DES were also performed.

1. Introduction

The effectiveness of LES as a practical method for predicting turbulent flows at high Reynolds numbers hinges on the fact that the grid density required to represent all influential dynamic processes rises modestly as $N \approx \mathrm{O}(Re^{0.4})$. However, this dependence applies only to regions that are remote from walls, where mixing is dictated by eddy length scales of order greater than 1–10% of the characteristic global dimension of the turbulent flow. Close to a wall, the dynamically influential energetic eddies progressively diminish in size as the wall is approached. Hence, if the near-wall region plays an important role in the behaviour of the flow properties of interest, the resolution requirements rise much more steeply with the Reynolds number. In a boundary layer or a channel flow, the influential near-wall structures feature directional length scales of size $\Delta y^+ = \mathrm{O}(1)$, $\Delta x^+ = \mathrm{O}(50)$, $\Delta z^+ = \mathrm{O}(20)$ (where x, y and z denote streamwise, wall-normal and spanwise directions, respectively). The need to maintain this aspect ratio approximately constant, irrespective of the Reynolds number, leads to the estimate (Chapman, 1979) that the grid size required to resolve the viscous sublayer rises in proportion to $Re^{1.8}$. This is close to the dependence $N \approx \mathrm{O}(Re^{2.25})$ demanded by DNS. Thus, the cost implications, even with an unstructured or nested wall-adaptive grid, become prohibitive at high Reynolds numbers.

The grid sensitivity of LES in near-wall flows is illustrated in Fig. 1 by the dramatic failure of a simulation for a channel flow at $Re = 42{,}200$ to reproduce the log-law in a fully-developed flow in a channel section of dimensions $2\pi h \times 2h \times \pi h$, covered by a typical wall-normal-clustered RANS-type grid of $64 \times 64 \times 32$ (denoted "LES coarse"), with the WALE model of Nicoud and Ducros (1999) used to represent subgrid-scale processes. Acceptable solution quality, with experimental results of Wei and Willmarth (1998) used as a benchmark, requires a grid more than an order of magnitude finer, as

* Corresponding author. Tel.: +44 207 594 5061; fax: +44 207 584 8120.
E-mail address: mike.leschziner@imperial.ac.uk (M.A. Leschziner).

0142-727X/$ - see front matter © 2004 Elsevier Inc. All rights reserved.
doi:10.1016/j.ijheatfluidflow.2004.07.006

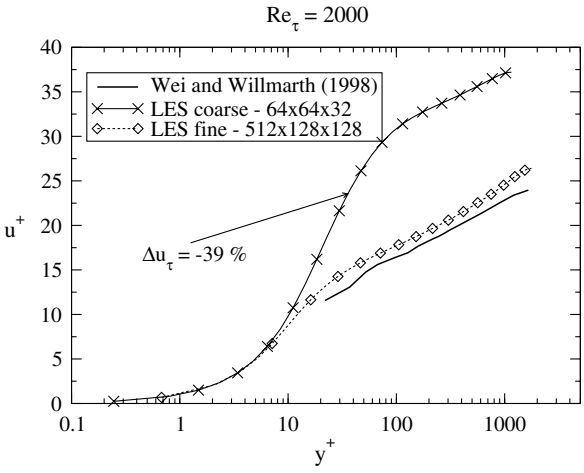

Fig. 1. Time-averaged velocity profiles obtained from LES at $Re_\tau = 2000$ for two different meshes.

illustrated in the same figure by a well-resolved LES with $512 \times 128 \times 128$ cells for a domain of size $2\pi h \times 2h \times \pi h/2$, satisfying the standard LES criteria for grid spacing.

Against the backdrop of the above observations, there is now a broad consensus that LES for practically relevant high-*Re* near-wall flows is only tenable in conjunction with near-wall approximations that permit a much coarser near-wall resolution to be adopted without the unacceptable penalties in accuracy demonstrated in Fig. 1. Two main approaches have been taken in recent years to this end. One involves the use of log-law- or power-law-based wall functions, similar to those adopted in RANS computations, to bridge the viscosity-affected sublayer. The other employs a RANS-type solution in the near-wall layer, with a low-Reynolds-number turbulence model. This solution either replaces the LES representation in the layer or is used to extract the wall-shear stress or a representative sublayer velocity, which is then fed into the LES solution as a boundary condition. Such two-layer or 'zonal' schemes pose a range of fundamental and practical questions, whatever approximation is adopted. At the most basic level, there arises the question of how to reconcile the filtering operation underlying the LES representation with the time-averaged framework on which RANS models are based or from which log-law-type approximations are derived. This conflict applies especially in the vicinity of the RANS–LES interface, where both the LES and RANS solutions resolve the same range of turbulent scales. Thus, in this region, the RANS model does not function as an integrator of even a modest range of scales which the simulation resolves.

The use of equilibrium-flow wall functions goes back to early proposals of Deardorff (1970) and Schumann (1975). A number of variations have subsequently been investigated, which are either designed to satisfy the log-law in the time-averaged field or, more frequently, involve an explicit log-law or closely related power-law prescription of the instantaneous near-wall velocity (e.g., Werner and Wengle, 1991; Hoffman and Benocci, 1995; Temmerman et al., 2003). These can provide useful approximations in near-equilibrium conditions, e.g., channel flow, but generally give a poor representation in non-equilibrium and separated flows in which the near-wall flow often lacks a distinct log-law region. Another unavoidable problem with wall-laws is that they do not return a credible representation of the variation of the flow properties and turbulence dynamics in the layer they bridge.

The alternative of adopting a RANS-type turbulence model for the near-wall layer is generally assumed to offer a more faithful representation of the near-wall flow at cell-aspect ratios much higher than those demanded by wall-resolved simulations. This is based on the observation that RANS calculations can give acceptable solutions for near-wall flows, especially in steady conditions, with cell-aspect ratios as high as 100–1000—a fact that is due, in large measure, to the low rate of change in the statistical properties parallel to the wall relative to that normal to it. However, in using any RANS model as a part of a hybrid LES–RANS strategy, it is observed that the level of the resolved motion in the near-wall RANS layer remains high. Thus, while the near-wall structure in this layer is, unsurprisingly, found to lack the small-scale features present in wall-resolving LES, the assumption of low rates of change in the wall-parallel directions is not valid. With the level of unsteadiness high in the inner layer, there also arises the question as to whether the closure assumptions, formulated for and calibrated by reference to steady flows, remain valid in highly unsteady straining. These are some of the many uncertainties surrounding LES/RANS hybrid strategies.

The best-known realisation of the hybrid concept is the DES method (Spalart et al., 1997). In this, the interface location is dictated by the grid parameters, through the switching condition $y_{\text{int}} = \min(y, C_{\text{DES}} \max(\Delta x, \Delta y, \Delta z))$. One and the same turbulence model, that of Spalart and Allmaras (1992), is used as a RANS model in the inner region and as a subgrid-scale model in the outer LES region. An important feature of this method is that it enforces the location of the RANS–LES switch at a y-location dictated, or at least strongly affected, by the *streamwise* and *spanwise* grid density. In general flows, this density often needs to be high to achieve adequate resolution of complex geometric and flow features, both close to the wall (e.g., in separation and reattachment regions) and away from it. Thus, the interface can be forced to be close to the wall, as near as $y^+ = \text{O}(20)$ at moderate values of the Reynolds number, defeating the basic rationale and objective of DES. Also, it has been repeatedly observed in conditions in which the interface is located at $y^+ = \text{O}(100\text{–}200)$, at high

Reynolds numbers and with coarse wall-parallel grids, that the high turbulent viscosity generated by the turbulence model in the near-wall region extends, as subgrid-scale viscosity, deep into the outer LES region, causing severe damping in the resolved motion and a misrepresentation of the resolved structure as well as the time-mean properties. This is conveyed by Fig. 2, which shows modelled and resolved contributions to the total shear stress of a DES computation for a channel flow at bulk Reynolds number of 42,200, using a $64 \times 64 \times 32$ ($N_x \times N_y \times N_z$) grid with cell dimensions $\Delta y^+ = 0.8$–222, $\Delta x^+ = 196$, $\Delta z^+ = 196$, for which the switching position occurs at $y^+ = 135$. An approach akin to DES, in the sense that a single RANS-type model is used throughout the whole flow domain, but with a continuous, *seamless* modification of the (subgrid-scale) model in the LES region, has been investigated by Hanjalić et al. (2004).

Zonal hybrid formations different from DES have been proposed and/or investigated by Balaras and Benocci (1994), Balaras et al. (1996), Cabot and Moin (1999), Wang and Moin (2000), Diurno et al. (2001) and Davidson and Peng (2001). In all but the last, unsteady forms of the boundary-layer (or thin-shear-layer) equations are solved across a near-wall layer of prescribed thickness, covered by a fine wall-normal mesh, with a van Driest mixing-length algebraic model providing the eddy viscosity. In the simplest form of the approach, this layer is pressure-decoupled from the LES region, with the pressure just outside the inner layer imposed across the layer, and advection is ignored. Cabot and Moin (1999) extended this thin-shear-layer approach by solving, simultaneously with the LES, the full parabolic momentum equations for the streamwise and spanwise velocity components, in which the turbulent shear stress components are again determined from a RANS-type mixing-length model. The principal quantity extracted from the RANS computation is the wall-shear stress or a velocity at a particular wall-normal distance, which is then fed into the LES solution as an unsteady boundary condition.

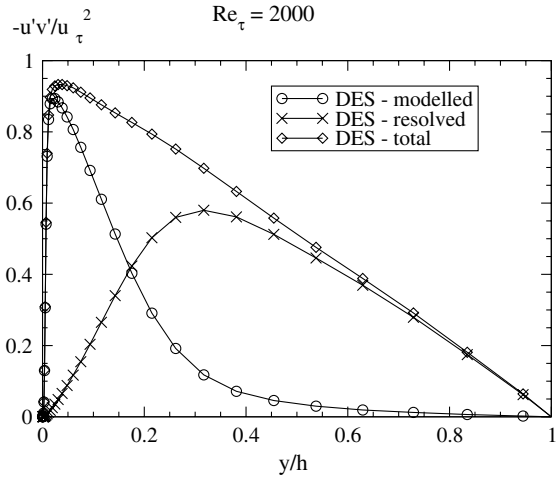

Fig. 2. Modelled and resolved contributions to shear stress predicted by DES in a channel at $Re_\tau = 2000$.

A practical problem that arises with virtually all forms of the hybrid approach is that they lack a mechanism for constraining the level of turbulence activity that arises in the RANS layer from a combination of model-produced eddy viscosity and the substantial resolved motion. It must be borne in mind that the eddy-viscosity provided by the turbulence model increases continuously away from the wall, without any constraint that imposes continuity in the turbulent/subgrid-scale viscosity and the associated stresses across the LES–RANS interface. The implication is that the time-averaged solution in the inner layer will not normally be compatible with the LES solution just outside the layer.

A final problem to point out here is the contradiction between the objective of assimilating the resolved dynamics into a statistical representation in the RANS layer and the requirement of retaining the small-scale motion close to the RANS–LES interface, in order to provide the outer region with the spectral perturbation that is necessary to sustain the correct turbulence dynamics in the LES domain. This physical inconsistency seems intractable in approaches based on simple merging, because the same equations are solved irrespective of whether they are filtered or time-averaged, and the modifications to subgrid-scale models reported in the literature generally fail to cure the problem. In an effort to compensate for the loss of small-scale motion caused by RANS-type near-wall modelling, Piomelli et al. (2003) have recently proposed the addition of extra spectral forcing to the RANS region. While this has been found to be beneficial, the nature of the forcing and the generality of the technique remain subjects for debate and continuing study.

In this paper, we investigate the characteristics of certain options for zonal or hybrid modelling without explicit spectral forcing. The methodology is targeted at any flow in which the turbulence processes in the sheared near-wall region exert a significant influence on the primary flow characteristics. In the first part, an a-priori study is undertaken to examine the ability of a representative one-equation (turbulence-energy) eddy-viscosity model to correctly represent the turbulent state in the near-wall layer as part of a LES approach. To this end, the near-wall layer is superimposed onto a full-field simulation, the latter providing 'boundary conditions' at the edge of the layer. Here, linkage is unidirectional, in the sense that the RANS layer receives the unsteady LES information, but does not feed back any information to the LES field. Thus, LES and unsteady RANS solutions are available simultaneously for the near-wall layer and can be compared in various ways. Of particular interest is the correspondence of the

combined modelled and resolved turbulence activity in the RANS layer to the wall-resolved LES state, and the mutual compatibility of conditions at the interface. In the second part of the paper, interface conditions are investigated within a fully coupled RANS–LES solution, and modifications are proposed to the turbulence model in the RANS layer, which ensure continuity across the interface. The characteristics of the resulting hybrid formulations are investigated by reference to simulations for fully-developed channel flow and a separated flow in a channel containing hill-shaped constrictions.

2. A-priori study

2.1. Methodology

A major uncertainty in the use of a RANS near-wall model within a LES scheme lies in the fundamental response of the former to the highly unsteady motion imposed on it by the latter at the interface. First, if that motion encompasses the entire turbulence spectrum, the sum of the modelled and the resolved transport can be expected to be excessive, at least in the vicinity of the interface where the RANS-resolved motion will necessarily be close to that imposed by the LES region. This misrepresentation is likely to be aggravated by the inapplicability of the underlying closure assumptions in the presence of intense unsteadiness, possibly giving rise to a wrong response of the stresses to the high rates of unsteady strains. Thus, the temporal response of the RANS model needs to be understood as a precursor to the introduction of any dynamic smoothing or filtering of the motion at the interface prior to its application to the RANS layer, or to a deliberate limitation of the modelled component. Second, as the RANS-resolved component decays towards the wall, with the modelled component dominating, structural features of turbulence are lost, and the correlation between the wall-shear stress and the motion away from the wall is lost too, or at least distorted. Thus, a possible consequence is that the wall shear stress—the key boundary condition—becomes seriously erroneous, at least in terms of its temporal behaviour. Both issues are investigated in the a-priori tests that follow.

The manner in which the tests have been conducted is conveyed, schematically, in Fig. 3. A near-wall RANS layer is superimposed onto the LES domain. The LES process is entirely unaffected by this overlay. The LES and RANS grids are identical in the overlap region. LES conditions are imposed at the interface plane, and the RANS equations are solved separately within the RANS region. Numerically, the layer is treated as a thin-shear-flow region, as done by Balaras et al. (1996). Thus, only the momentum equations for the wall-parallel velocity components are solved, with the unsteady pressure and wall-parallel velocity components taken from the LES and imposed at the RANS-layer boundary. The wall-normal velocity is determined by applying the continuity equation directly to the near-wall finite-volume cells, starting at the lower wall. An inevitable consequence of this simplification is a discontinuity between the RANS and LES wall-normal velocity components at the RANS-layer boundary. This is the source of some uncertainty in the evaluation of the resolved stresses involving wall-normal fluctuations, but is otherwise likely to be of little consequence.

The LES procedure itself is based on a general co-located, cell-centred, finite-volume scheme and a second-order fractional-step solution method within which the pressure equation is solved by Fourier-based (spanwise) partial-diagonalisation combined with multigrid relaxation (Temmerman et al., 2003).

The study is undertaken for a plane, fully-developed channel flow at $Re_b = 10{,}935$, over a domain of $2\pi h \times 2h \times \pi h$, where h is the channel half height. Unless otherwise stated, the grid used consists of $96 \times 64 \times 64$ nodes, with the wall-nearest nodal plane located at $y^+ \approx 1$. The interface is placed 13 nodal planes away from the wall at $y^+ \approx 65$. This value is typical for the location at which one would wish to see the RANS layer take over the resolution of the near-wall region. It is of interest to note here that the application of the DES hybrid approach in the present flow conditions and with the same grid results in coupling at $y^+ = 24$, i.e. very close to the wall. Coarsening the grid in the streamwise or spanwise directions, precisely the option one wants to

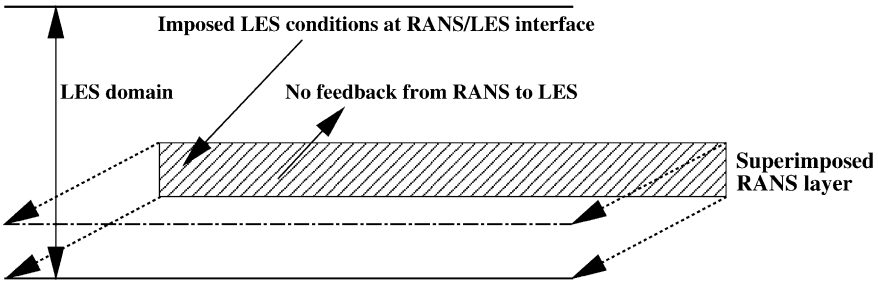

Fig. 3. Schematic of RANS/LES overlap.

exploit in a hybrid scheme, leads to higher values, but as the interface y^+ value increases, the solution quality around the interface deteriorates rapidly.

The LES solution is obtained with the Smagorinsky (1963) SGS model (with constant $C_s = 0.1$) in combination with the wall-damping function:

$$f_{v,\mathrm{SGS}} = 1 - \exp\left(\frac{y^+}{5}\right) \tag{1}$$

which procures the required decay of the SGS viscosity in the viscous sublayer. This is not a particularly good SGS model, however, and will be seen to return rather indifferent agreement with DNS data, especially in the buffer region.

The RANS model chosen for the present study is the one-equation model of Wolfshtein (1969):

$$\frac{\partial k_{\mathrm{RANS}}^{\mathrm{mod}}}{\partial t} + \frac{\partial u_j k_{\mathrm{RANS}}^{\mathrm{mod}}}{\partial x_j} = \frac{\partial}{\partial x_j}\left(\left(\nu + \nu_{\mathrm{RANS}}^{\mathrm{mod}}\right)\frac{\partial k_{\mathrm{RANS}}^{\mathrm{mod}}}{\partial x_j}\right) + P_k - \frac{k_{\mathrm{RANS}}^{\mathrm{mod}\ 1.5}}{l_\epsilon} \tag{2}$$

$$\nu_{\mathrm{RANS}}^{\mathrm{mod}} = C_\mu k_{\mathrm{RANS}}^{\mathrm{mod}\ 0.5} l_\mu \tag{3}$$

$$l_\mu = C_l(1 - \exp(-0.016y^*))$$

$$l_\epsilon = C_l(1 - \exp(-0.263y^*)) \quad \text{with} \quad y^* = \frac{y k_{\mathrm{RANS}}^{\mathrm{mod}\ 0.5}}{\nu} \tag{4}$$

The use of a model involving an explicit length-scale prescription, whilst restrictive in terms of generality, is convenient, in so far as it obviates the need to prescribe a boundary condition for a length-scale surrogate (e.g., ϵ, ω) which is governed by a related transport equation within a more general framework considered later. This is a significant problem posed by any two-equation model, since a coarse-grid LES cannot provide reliable values for ϵ or ω. Here, the only interface quantity needed is k. A reasonable choice, consistent with continuity in the resolved motion across the interface, is:

$$k = k_{\mathrm{LES}}^{\mathrm{mod}} = 0.5\overline{u_i'}\,\overline{u_i'}, \quad \overline{u_i'} = \overline{u_i} - \widehat{\overline{u_i}} \tag{5}$$

where $\bar{\cdot}$ denotes grid filtering, and $\hat{\cdot}$ identifies test filtering, in the sense of dynamic SGS modelling, over the test filter $\widehat{\overline{\Delta}} = 2\overline{\Delta}$.

2.2. Results

The first a-priori test examines the wall-normal variation of the correlation coefficients $\langle u'u_\tau'\rangle/u_{\mathrm{rms}}u_{\tau,\mathrm{rms}}$ and $\langle \alpha'\beta'\rangle/\alpha_{\mathrm{rms}}\beta_{\mathrm{rms}}$, where both arise either from the LES or RANS solution, u_τ is the wall-shear velocity, $\alpha = \mathrm{angle}(0,\mathbf{u_{xz}})$, $\beta = \mathrm{angle}(0,\boldsymbol{\tau_w})$ and $\langle\cdot\rangle$ identifies time-averaging. Both are two-point correlations, examining how the wall-parallel motion at y is correlated, in terms of magnitude and angle, with the wall-shear stress. This is done for both the RANS solution and the solution returned by the LES within this layer. A comparison of the y-wise variation of both correlations is given in Fig. 4. This conveys information on the extent to which the RANS model preserves key statistical parameters associated with the unsteady motion in the near-wall layer. The correlations are also of interest in relation to the use of wall laws in approximating the near-wall region, for, evidently, wall laws establish (inappropriately) a perfect correlation between the motion at the outer edge of the wall-law region and the wall shear stress.

As is evident from Fig. 4, the RANS model represents (surprisingly) well the correlation levels predicted by the LES solution. This is recognised, qualitatively, in Fig. 5 which gives the time histories of the velocity at $y^+ = 30$ and the wall-shear velocity. These results suggest a substantial unsteady motion throughout the RANS region. Clearly, the unsteady LES motion imposed at the RANS-layer edge decays only slowly through the RANS region, and this has important implications for what is the appropriate level of the modelled viscosity in the RANS layer, especially close to the interface.

Next, time-averaged properties are examined. In a preliminary test, not included here, a steady solution was obtained with the Wolfshtein model by applying it across the entire channel. This solution was generated

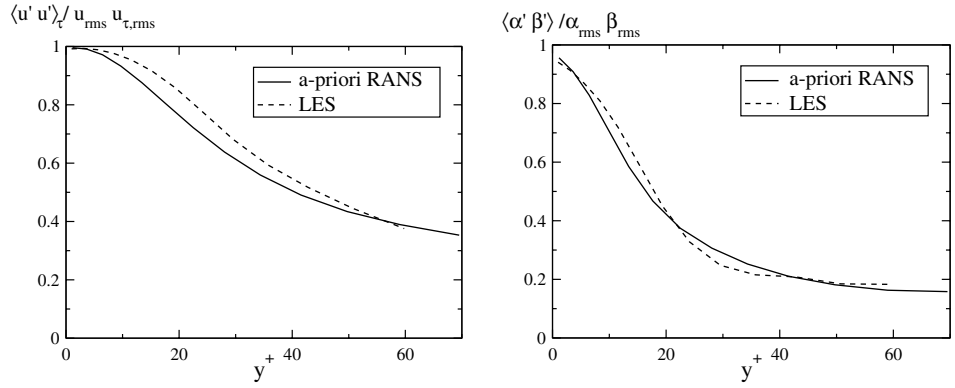

Fig. 4. Wall-normal variations of the correlations for the a priori RANS and the equivalent LES.

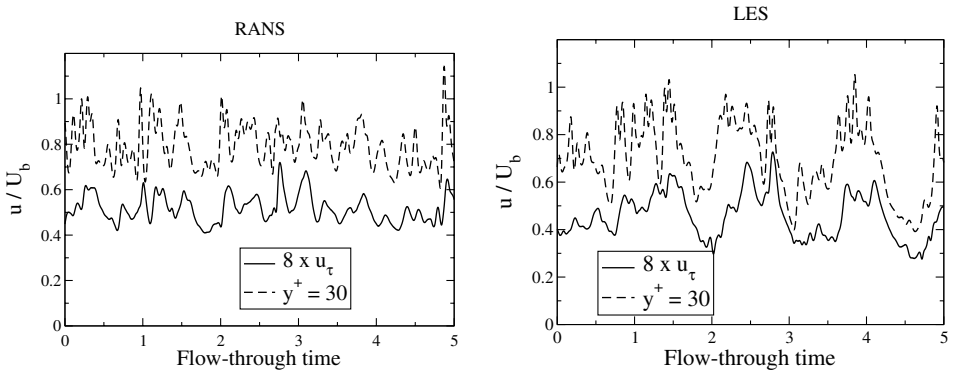

Fig. 5. Time history for the velocity ($y^+ = 30$) and wall-shear velocity for the a priori RANS and the equivalent LES.

by the LES code in which the SGS model was replaced by the Wolfshtein model, thus suppressing unsteady motion and yielding a steady RANS solution. The test verified the correctness of the model's implementation, although agreement with the DNS solution was not especially close, pointing to model defects, at least in low-*Re* channel flow. Fig. 6 compares the time-averaged velocity profile resulting from DNS, the present LES and the RANS scheme in the near-wall region. The pure LES solution is seen to be rather poor in the buffer region, relative to DNS, and this is a consequence of the use of the wall-damped Smagorinsky model which does not return the requisite y^{+3} near-wall decay of the SGS viscosity. The RANS model returns a profile that is flatter than the LES profile and also an excessive wall-shear stress, thus suggesting a higher level of turbulence and shear stress than that implied by the LES. This is indeed the case, as is confirmed by Fig. 7a which shows turbulence-energy profiles. The figure includes the resolved and modelled components of both LES and RANS solutions, the modelled LES component $k_{\mathrm{LES}}^{\mathrm{mod}}$ being estimated from (5). As expected, the last is a rather small contribution relative to the resolved component, except in the buffer layer. In contrast, the RANS-modelled component of both shear stress and turbulence energy are much larger contributors to the respective totals. At the same time, the resolved RANS components are substantial—not much lower than the resolved LES components—and this results in excessive total shear stress and especially turbulence energy. Consistently, as shown in Fig. 7b, the eddy-viscosity derived from the RANS-predicted time-averaged total shear stress and strain is considerably larger that the corresponding level derived from the LES solution.

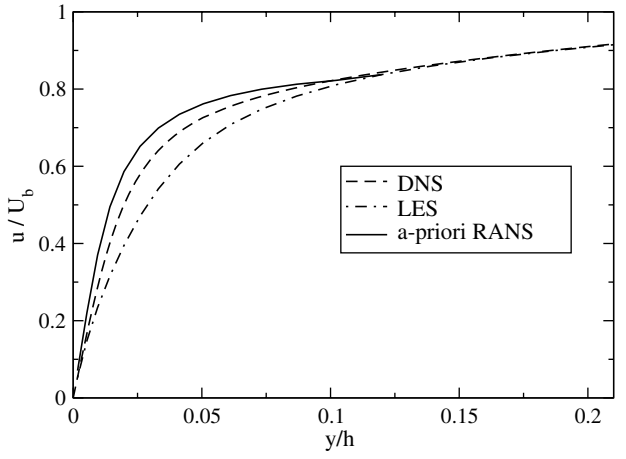

Fig. 6. Time-averaged velocity profiles for the reference DNS, the a priori RANS and the equivalent LES.

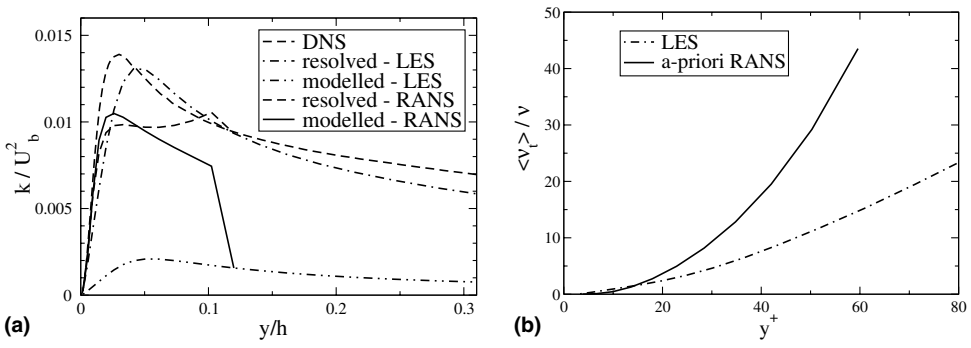

Fig. 7. (a) Turbulence-energy profiles for the a priori RANS and the equivalent LES in comparison to DNS. (b) Total (modelled + resolved) eddy-viscosity profiles for the a priori RANS and the equivalent LES.

Thus, the picture emerging from the tests is that the RANS framework, when implemented in its default form, provides a seriously excessive level of turbulence transport in the near-wall layer. This is expected to apply to virtually all models, at least those which are based on the eddy-viscosity form and do not involve any specific corrections.

3. A two-layer hybrid scheme

3.1. Matching criteria

The results introduced in the previous section illustrate that the RANS approach returns turbulence energy, viscosity and shear-stress levels that are substantially higher than those resulting from the LES solution. This clearly suggests a potentially serious incompatibility at the interface, which requires resolution by the imposition of some limiting criteria. These must be such that the disparate approaches to modelling the RANS and subgrid-scale viscosities can be reconciled.

A procedural advantage of the DES method is that it uses a single framework, the Spalart-Allmaras (SA) model, to determine the viscosity on both sides of the RANS–LES interface, with the length scale tied to the wall distance in the RANS region and to the maximum cell dimension in the LES region, both matching at the interface. While this grid-controlled switching avoids interface discontinuities, some disadvantageous consequences of this practice arise and have been pointed out in Section 1. The a-priori tests in the previous section are pertinent to these defects, for they indicate clearly that the use of an unmodified RANS model in the near-wall region—and this must be assumed to include the SA model—would give an excessive viscosity in the RANS layer as well as in the LES region adjacent to the interface if used in DES mode, unless the flow in the near-wall layer is steady. It thus follows that the DES method also requires (or would benefit from) some form of dynamic adjustment of the type proposed below.

In one zonal-modelling option by the present authors (Temmerman et al., 2003), a one-equation turbulence-energy model is solved in both the RANS and LES sub-domains. The RANS and subgrid-scale models differ only in the manner in which the dissipation rate and eddy viscosity are defined. In the RANS region, the model of Wolfshtein (1969) or, alternatively, that of Norris and Reynolds (1975) is used for the length scales which occur in the model relations for the dissipation and eddy viscosity. In the LES region, the subgrid-scale model of Yoshizawa and Horiuti (1985) is used. The two methods are bridged at the interface by interchanging velocities, modelled turbulence energy and turbulent viscosity, the last subject to the continuity constraint across the interface:

$$\nu_{\mathrm{LES}}^{\mathrm{mod}} + \nu_{\mathrm{LES}}^{\mathrm{res}} = \nu_{\mathrm{RANS}}^{\mathrm{mod}} + \nu_{\mathrm{RANS}}^{\mathrm{res}} \tag{6}$$

where the resolved LES viscosity may be extracted from:

$$\nu_{\mathrm{LES}}^{\mathrm{res}} = \frac{\langle \overline{u_i' u_j'}^{\mathrm{res}} \overline{S_{ij}} \rangle}{\langle \overline{S_{ij}} \overline{S_{ij}} \rangle} \tag{7}$$

with the overbar identifying filtered quantities and $\langle\,\rangle$ denoting averaging over any homogeneous direction (or both, in plane channel flow) or over some pre-defined patch on both sides of the interface. The alternative of using local (non-averaged) quantities is discussed below. The constraint (6) is met by forcing the coefficient C_μ in the RANS eddy-viscosity model to take an interface value consistent with the condition:

$$\langle \nu_{\mathrm{LES}}^{\mathrm{mod}} \rangle = C_{\mu,\mathrm{int}}^{\mathrm{av}} \langle (k_{\mathrm{RANS}}^{\mathrm{mod}})^{1/2} l \rangle \tag{8}$$

The smooth transition from the RANS value $C_\mu = 0.09$ to the interface value $C_{\mu,\mathrm{int}}$ is effected by the empirical exponential function:

$$C_\mu = 0.09 + (C_{\mu,\mathrm{int}} - 0.09) \frac{1 - \exp(-y/\triangle)}{1 - \exp(-y_{\mathrm{int}}/\triangle_{\mathrm{int}})} \tag{9}$$

which is one of several options investigated, where "int" denotes the interface location. There is no obvious physical justification for this functional dependence; it is a proposed prescription. However, it will be shown below, on the basis of a-posteriori testing, that this type of variation is appropriate.

The recognition that the imposition of a static length scale is unrealistic and likely to be a source of error has led to the extension of the above approach to two-equation modelling in the RANS layer. The particular model selected for this extension is that of Abe et al. (1994). The turbulent viscosity is then given by:

$$\nu_t = C_\mu f_\mu k^2/\varepsilon \tag{10}$$

where f_μ is a damping function which is part of the model. Hence, $C_{\mu,\mathrm{int}}$ now arises from Eq. (10) and Eq. (7) as:

$$C_{\mu,\mathrm{int}}^{\mathrm{av}} = \frac{\langle \nu_{\mathrm{LES}}^{\mathrm{mod}} \rangle}{\langle f_\mu k^2/\varepsilon \rangle} \tag{11}$$

where $\langle \cdot \rangle$ means, as before, averaging over homogeneous directions.

The solution of the RANS model now requires the specification of boundary conditions for k and ε at the RANS/LES interface. When a k-equation-based subgrid-scale model is used, this provides the sub-grid-scale energy, hence yielding the required boundary value for k, while ε may be evaluated from $k^{3/2}/C_l y$. For more complex flows, where the characteristic wall distance is not clearly defined, this may pose a problem, however. Some of the results presented below were obtained with a *dynamic* sub-grid-scale model which does not provide

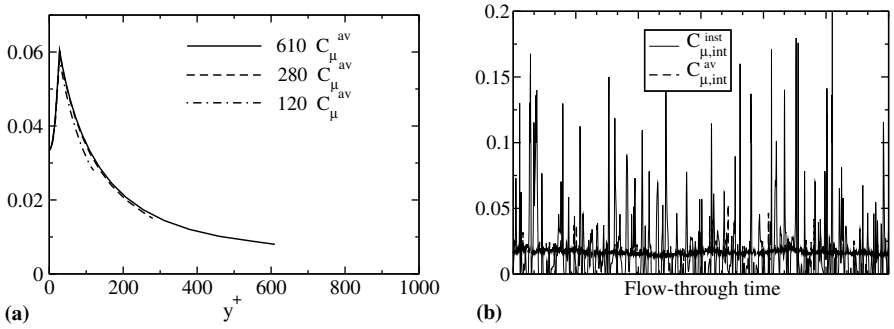

Fig. 8. (a) Variation of (time-invariant) C_μ across the flow. (b) Histograms of the instantaneous and homogenously-averaged C_μ at the RANS/LES interface.

explicitly the sub-grid-scale energy. Rather, this is estimated, based on similarity arguments, from Eq. (5).

Preliminary testing with the above RANS model revealed the original proposal for C_μ by Temmerman et al. (2003) to produce excessive modelled turbulent viscosity in the near-wall region, up to $y^+ = 25$, and this was therefore modified to the following form:

$$C_\mu = \begin{cases} \frac{15.0}{40.0-y^+}\left(0.09 + (C_{\mu,\mathrm{int}} - 0.09)\frac{1-\exp(-y/\triangle)}{1-\exp(-y_{\mathrm{int}}/\triangle_{\mathrm{int}})}\right), \\ \quad \text{if } y^+ < 25 \\ 0.09 + (C_{\mu,\mathrm{int}} - 0.09)\frac{1-\exp(-y/\triangle)}{1-\exp(-y_{\mathrm{int}}/\triangle_{\mathrm{int}})}, \\ \quad \text{if } y^+ > 25 \end{cases} \tag{12}$$

The variation of C_μ, derived from Eqs. (11) and (12) for three different interface locations is shown in Fig. 8a. The distributions illustrate that, depending on the location of the interface, the implied interface C_μ, in this case extracted from the dynamic model, can be as low as 0.01. Fig. 8b demonstrates that the instantaneous value varies greatly in time, reflecting the presence of high-frequency perturbations on the LES side. Thus, the use of an averaged value clearly filters out, possibly to a substantial degree, the transmission of perturbations to the RANS layer. To investigate the impact of this filtering, and in an attempt to introduce a more faithful spectral representation into the RANS layer, tests were also conducted with *instantaneous* values of $C_{\mu,\mathrm{int}}^{\mathrm{inst}} = \nu_{\mathrm{LES}}^{\mathrm{mod}}/(f_\mu k^2/\varepsilon)$ imposed at the interface. The consequences of this variation will be discussed below, as part of an extensive range of studies testing the effectiveness of the practices outlined above.

3.2. Results for channel flow

3.2.1. One-equation model

The performance of variants of the present LES/RANS hybrid method is conveyed in this section by way of solutions for channel flow at $Re_\tau = 590$ and 2000. The latter corresponds to a bulk Reynolds number of 42,200, and is considered high enough to convey the essential characteristics of the method. A constraint on the Reynolds number is also posed by the cost of generating accurate, wall-resolved LES solutions against which to contrast those derived from the hybrid scheme.

A first set of solutions, obtained with the combination of Wolfshtein's one-equation model, Eq. (2) to Eq. (4) in the RANS layer, the one-equation subgrid-scale model of Yoshizawa and Horiuti (1985) and matching relation (9), are presented in Figs. 9–13. At the lower Reynolds number, the interface is placed at $y^+ = 65$, while two locations, $y^+ = 48$ and 135, denoted I.1 and I.2, respectively, in figures to follow, have been examined at the higher Reynolds number. The computations have been compared to DES results for identical conditions and meshes, but only a few of these results are included herein because of space constraints. Hybrid RANS/LES solutions are identified by "HRL". Four meshes are used: M1 and M2 for $Re_\tau = 590$ and M3 and M4 for $Re_\tau = 2000$:

- M1: $Nx \times Ny \times Nz = 64 \times 64 \times 32$ with cell dimensions $\Delta y^+ = 2$–42, [1] $\Delta x^+ = 58$, $\Delta z^+ = 58$, used for DES and HRL at $Re_\tau = 590$;
- M2: $96 \times 64 \times 64$ with cell dimensions $\Delta y^+ = 2$–42, $\Delta x^+ = 38$, $\Delta z^+ = 29$, used for LES at $Re_\tau = 590$;
- M3: $64 \times 64 \times 32$ with cell dimensions $\Delta y^+ = 0.8$–222, $\Delta x^+ = 196$, $\Delta z^+ = 196$, used for DES and HRL at $Re_\tau = 2000$;
- M4: $512 \times 128 \times 128$ with cell dimensions $\Delta y^+ = 1.5$–86, $\Delta x^+ = 24.5$, $\Delta z^+ = 24.5$, used for LES at $Re_\tau = 2000$.

Meshes M2 and M4 are appropriate for wall-resolving LES at the respective Reynolds numbers. Meshes M1 and M3, used for the DES and HRL computations, have an aspect ratio $\Delta x^+/\Delta z^+ = 1$, in adherence with a recommendation by Shur et al. (1999), and these would

[1] The lower figure in the range 2–42 applies to the wall, while the higher applies to the centre plane. Note also that the grid node closest to the wall is located at $y^+ = 1$.

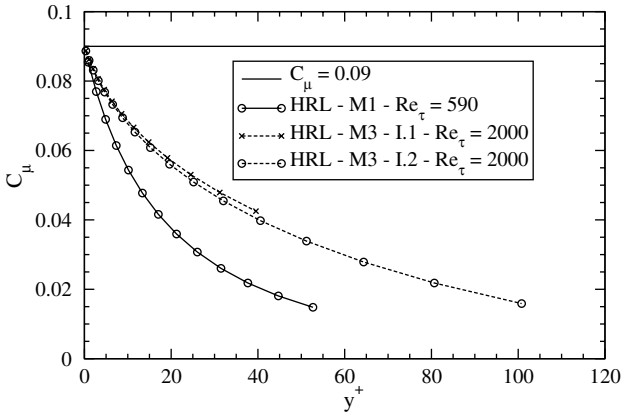

Fig. 9. Time-averaged C_μ profiles across the RANS layer for two different Reynolds numbers.

be of the type and density appropriate to RANS computations of evolving near-wall shear flows. While meshes M3 and M4, used for the higher Reynolds number, differ greatly, M1 and M2 are similar, reflecting limitations on a reduction of the streamwise and spanwise resolution below a level at which the LES would not able to capture even the most important scales in the outer region. The meshes used for the LES computations are expected to provide a reasonably good resolution and adhere to standard meshes often used in the literature.

Fig. 9 shows the C_μ distributions represented by relation (9) generated with meshes M1 and M3 for $Re_\tau = 590$ and 2000, respectively. The interface value computed from the LES solutions are about 0.015, close to that arising from the dynamic model (see Fig. 8a). At the higher Reynolds number, it is interesting to observe that the C_μ value computed when the interface is shifted from $y^+ = 135$ (I.2) to 48 (I.1) agrees closely with relation (9). It is not surprising, therefore, to observe in comparisons to follow that the two solutions with the two interface locations for $Re_\tau = 2000$ also agree well.

Figs. 10–13 present, respectively, comparisons for mean velocity, shear stress, turbulence energy and turbulent/SGS viscosity. The comparisons includes HRL, DES and wall-resolved simulations. LES solutions have been obtained both on the LES grids and on the DES/HRL grids, the latter to illustrate the poor quality of LES on the coarser grids used in conjunction with the RANS layer. Where appropriate, the position of the LES/RANS interface is indicated on plots by vertical lines.

It is instructive to start with a consideration of the eddy/SGS viscosity distributions, shown in Fig. 13. First, it is observed from the r.h.s. plots that the SGS viscosity levels returned by the SGS model in the wall-resolved LES computations are very low, of order 0.5 times the fluid viscosity. Thus, the LES solutions on grids M2 and M4, presented in Figs. 11–13, reflect,

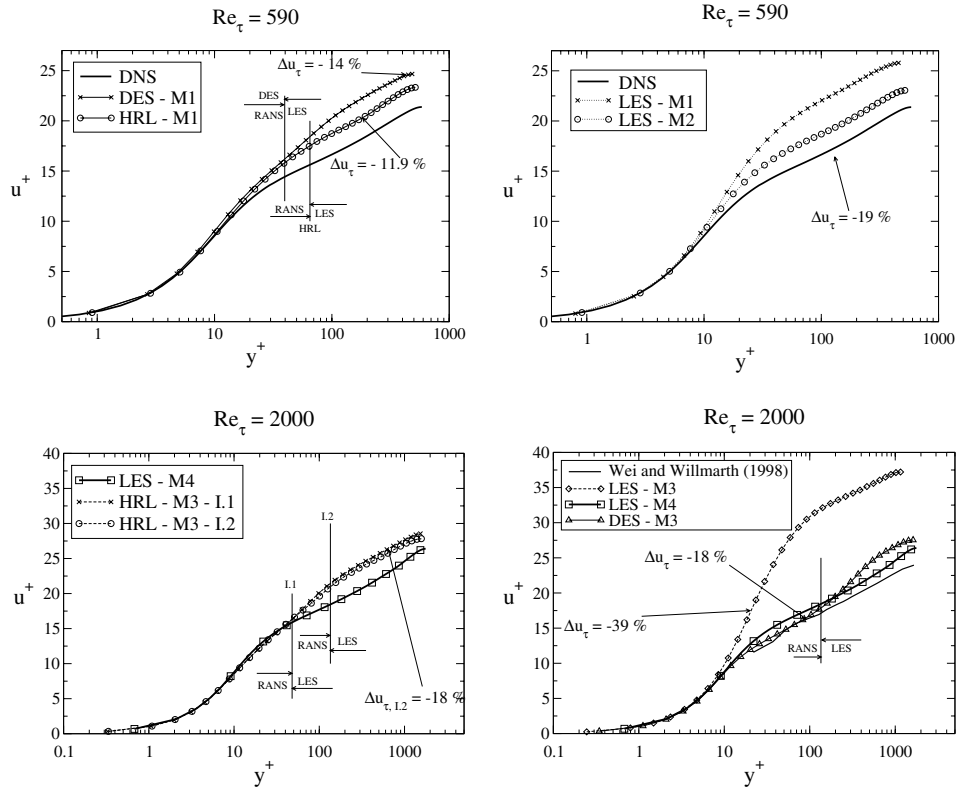

Fig. 10. Time-averaged velocity profiles for the references, HRL, DES and LES.

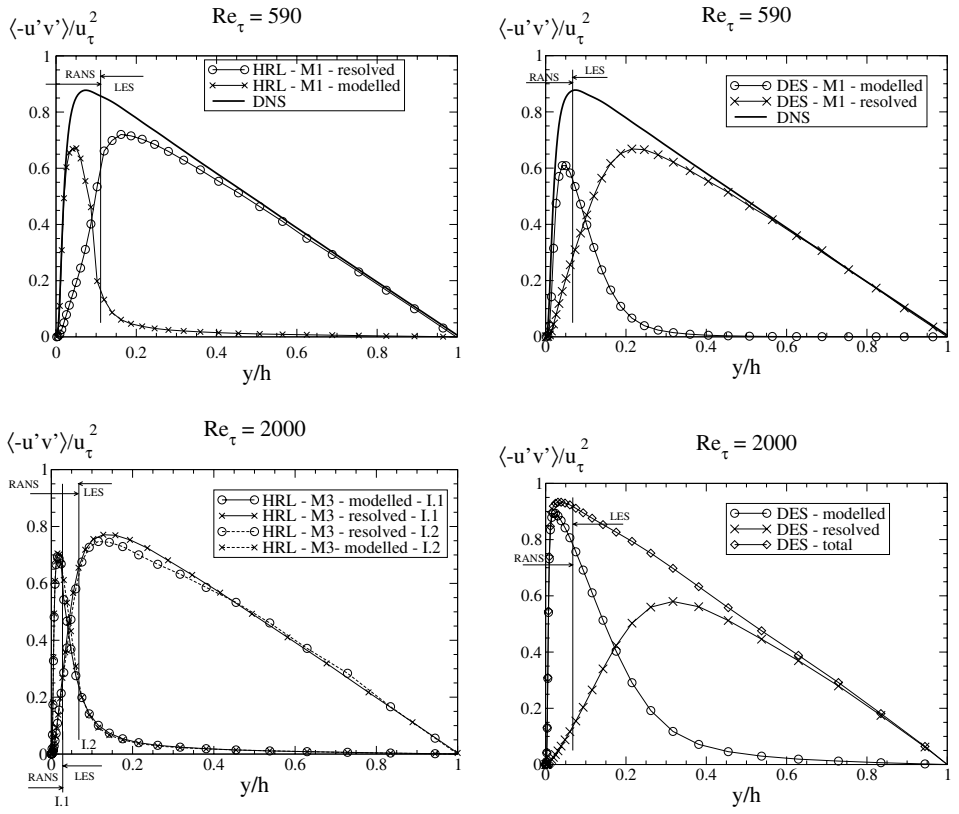

Fig. 11. Shear-stress profiles for the references, HRL and DES.

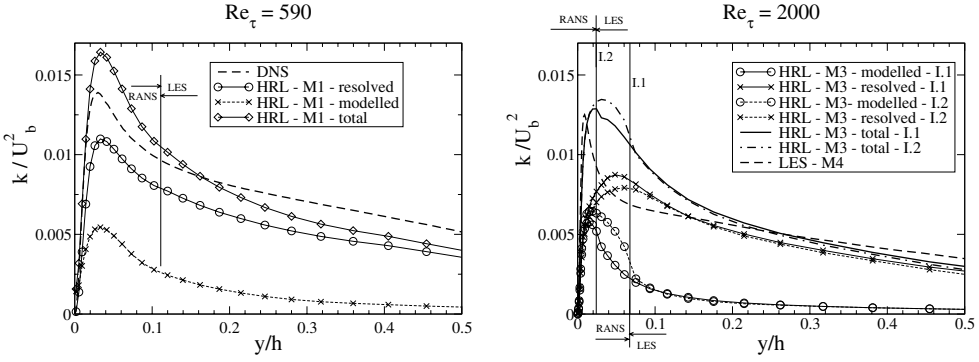

Fig. 12. Turbulence energy profiles for the references, HRL (modelled, resolved and total).

almost entirely, the resolved motion, any errors being due, essentially, to resolution limitations. In the DES simulations on grids M1 and M3, the y^+-locations at which the switch occurs from the RANS to the LES scale are 36 and 120 for $Re_\tau = 590$ and 2000, respectively. As seen, the DES-produced viscosity is not merely very high in the RANS region, but this high level is also maintained over a substantial portion of the LES domain. Indeed, the modelled viscosity exceeds the equivalent resolved level (i.e. that arising from $\langle u'v' \rangle_{\text{resolved}} / \langle \partial u / \partial y \rangle$) within $y^+ = 110$ for $Re_\tau = 590$ and $y^+ = 500$ for $Re_\tau = 2000$, respectively. This behaviour is remarkable and explains the observation that, at high Reynolds numbers, the condition in the turbulent near-wall layer is dominated by the modelled viscosity; in other words, the outcome is a RANS-type solution, rather than one that arises from a conventional simulation. In marked contrast to the DES results, those for the present HRL practice indicate that the model-induced elevation in viscosity is both highly confined to the near-wall region and much lower than the DES value, typically by a factor 4 in terms of the maximum value.

Fig. 10 shows first (r.h.s. column) that the predicted LES solutions on the LES grids M2 and M4 agree fairly well with benchmark DNS or experimental results of Wei and Willmarth (1998). However, when LES simula-

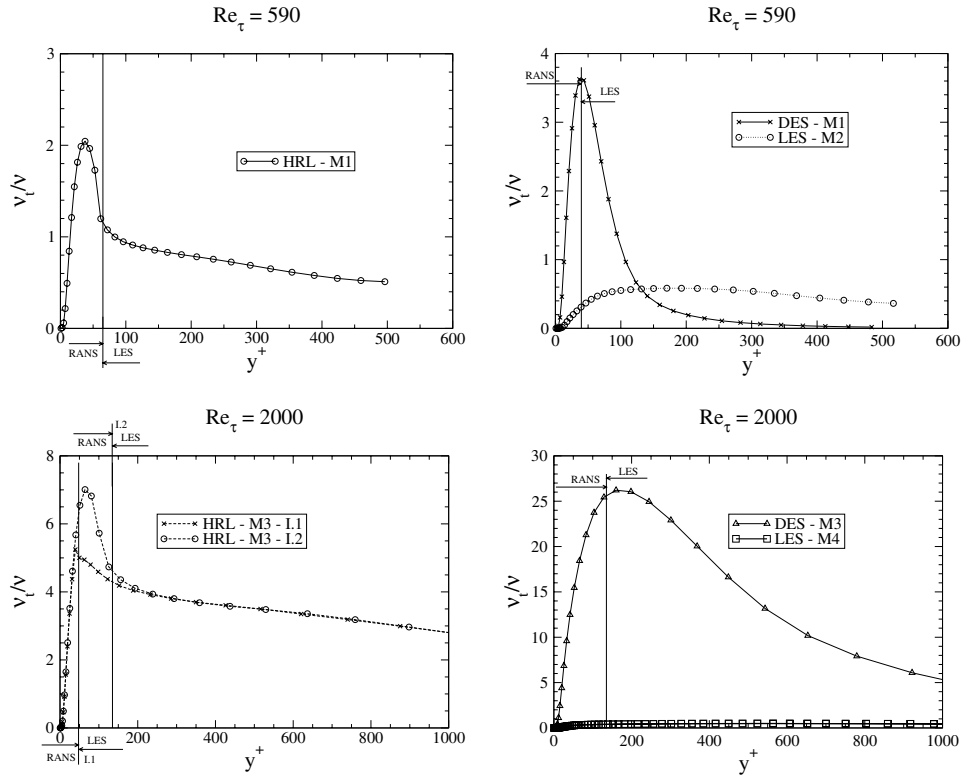

Fig. 13. Modelled viscosity profiles for HRL, DES and LES.

tions are performed on the grids M1 and M3, the results are (unsurprisingly) poor—indeed, extremely poor in the case of $Re_\tau = 2000$. This is a stark demonstration of the resolution challenges LES faces in high-Reynolds-number flows. The present HRL method gives substantially better results than the pure LES on the coarser grids, although differences relative to the reference distributions remain.

The variations of resolved and modelled contributions to the shear stress, shown in Fig. 11, are qualitatively consistent with observations already made in relation to the viscosity. The LES solutions on the wall-resolving meshes M2 and M4 are not included, but have been found to give, as expected, insignificant subgrid-scale contributions. Especially at the higher Reynolds number, the DES method (r.h.s. column) produces a much higher level of modelled contribution, over a much larger extent of the near-wall region, relative to the HRL approach (l.h.s. column), and this is in agreement with the trends shown in Fig. 13.

Turbulence-energy distributions are included in Fig. 12 only for the HRL solutions, relative to the reference LES profiles, in order to identify the extent to which the dynamic RANS-model adjustment suppresses the excessive energy levels otherwise observed. Given are the resolved and modelled contributions as well as the total energy. For both Reynolds numbers, the HRL-produced totals are seen to exceed the corresponding reference levels for some distance beyond the buffer region, but the maxima are similar, and the agreement is broadly satisfactory, considering the challenge.

Although normal-stress distributions are not included herein, it is appropriate to remark that the differences between DES and HRL representations have been observed to be especially large in respect of the anisotropy. Because of the dominance of the isotropic RANS model in the DES simulation, the method is unable to give a credible representation of the anisotropy over a substantial proportion of the near-wall layer. In contrast, the far lower relative contribution of the RANS model in the HRL method allows the simulations to give a credible representation of anisotropy, which compares well with the highly-resolved LES solution.

3.2.2. Two-equation model for the RANS region

Considered next are results for the channel flow at $Re_\tau = 2000$, obtained with the two-equation RANS model described in Section 2 and the dynamic subgrid-scale model in the LES domain. Figs. 14a–c show, respectively, variations of time-averaged velocity, turbulent viscosity and turbulent shear stress (the modelled component as well as the total) obtained on mesh M3 with Eqs. (10) and (11) in the RANS layer and the matching condition (12). To examine the sensitivity of the solution to the interface location, simulations were undertaken for y^+_{int} varying between 120 and 610. The

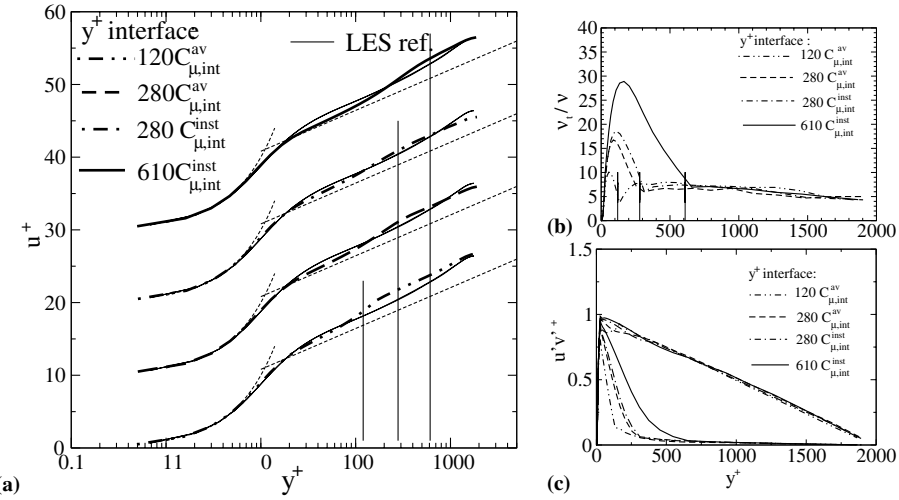

Fig. 14. Zonal RANS/LES results for different interface locations. (a) Mean velocity. (b) Modelled eddy viscosity (normalized with ν). (c) Total and modelled turbulent shear stress.

simulations were performed both with averaged and instantaneous implementations of Eq. (10), identified by "C_μ^{aver}" and "C_μ^{inst}", respectively.

The use of the two-equation model is observed to lead to some predictive improvements in respect of the velocity relative to the one-equation model, partly because of the modifications to C_μ, but also because the length-scale variable, here ε, is allowed to respond to external perturbations via its own transport equation. However, the anomaly around the interface, observed earlier and attributed to insufficient effective viscosity in this region, is seen in Fig. 14 to persist. Imposing *instantaneous* values of $C^{\text{inst}}_{\mu,\text{int}} = \nu^{\text{mod}}_{\text{LES}}/(f_\mu k^2/\varepsilon)$ at the interface (see Fig. 8b) introduces high-frequency components at this interface, and this is observed in Fig. 14 to diminish the unphysical inflection in the velocity profile around the interface. Although this option cannot be claimed to generate realistic streaks and other missing small-scale structures that are inevitably inaccessible to URANS, it seems that the use of $C^{\text{inst}}_{\mu,\text{int}}$ provides some desirable extra unsteady forcing, thus injecting a proportion of the missing high-frequency components and improving the effective eddy viscosity. Beneficial effects arising from artificial forcing in the vicinity of the interface have also been reported by Piomelli et al. (2003) who introduced a randomly generated "stochastic backscatter" at an intensity dependant on the wall-distance. The present use of $C^{\text{inst}}_{\mu,\text{int}}$ is similar in spirit, but is procedurally simpler and more natural.

As is observed in Fig. 14, placing the interface closer to the wall results, in accord with expectation, in an increase of the resolved stresses and decrease in the eddy viscosity. However, the eddy viscosity shows a rather discontinuous behaviour, with the viscosity dropping rapidly as the interface is approached, thus resulting in an excessive velocity gradient in this region. As the interface is moved away from the wall, the results improve, the variation of eddy viscosity becomes more gradual, and the velocity profile is smoother. The predicted friction factor also improves, with an error of 9% for $y^+_{\text{int}} = 120$, with $C^{\text{av}}_{\mu,\text{int}}$, diminishing to 3.3% for $y^+_{\text{int}} = 610$ with $C^{\text{inst}}_{\mu,\text{int}}$. In essence, by increasing the near-wall layer, a heavier burden is placed on the RANS model, and the role of LES in the outer region is progressively reduced to capturing only the very large structures in the channel-core region and thus providing unsteady forcing to the RANS region, rather than returning the true and complete large-scale turbulence spectrum. This is conveyed qualitatively by Fig. 15 which shows contours of instantaneous streamwise vorticity in a cross-flow plane. Fig. 15a, corresponding to $y^+_{\text{int}} = 120$ and $C^{\text{av}}_{\mu,\text{int}}$, contains elements of typical streaky near-wall structures, with streak centres at around $y^+ = 70$. However, because of the coarse spanwise mesh spacing ($\Delta z^+ \approx 200$), the streaks are much wider ("superstreaks"), and their distance is much larger ($z^+ = 500$) than in reality, represented by the highly-resolved LES result shown in Fig. 15d. The interface at $y^+ = 120$ cuts through the middle of the streaks-populated region, which also partly explains the source of the interface anomaly in the mean velocity. Moving the interface closer to the wall evidently leads to a greater proportion of the small-scale structures being captured. However, reproducing faithfully the streak topology would require the grid to be refined substantially, especially in the spanwise direction, thus departing from the main motivation for the hybrid approach. On the other hand, as the interface is placed further from the wall, the streaky pattern becomes progressively indistinct, although for $y^+ = 280$, this pattern is still visible, partly because $C^{\text{inst}}_{\mu,\text{int}}$ has been used in this case, as opposed to $C^{\text{av}}_{\mu,\text{int}}$ in Fig. 15a. The streak centres shift further from the wall to about $y^+ = 100$, but their

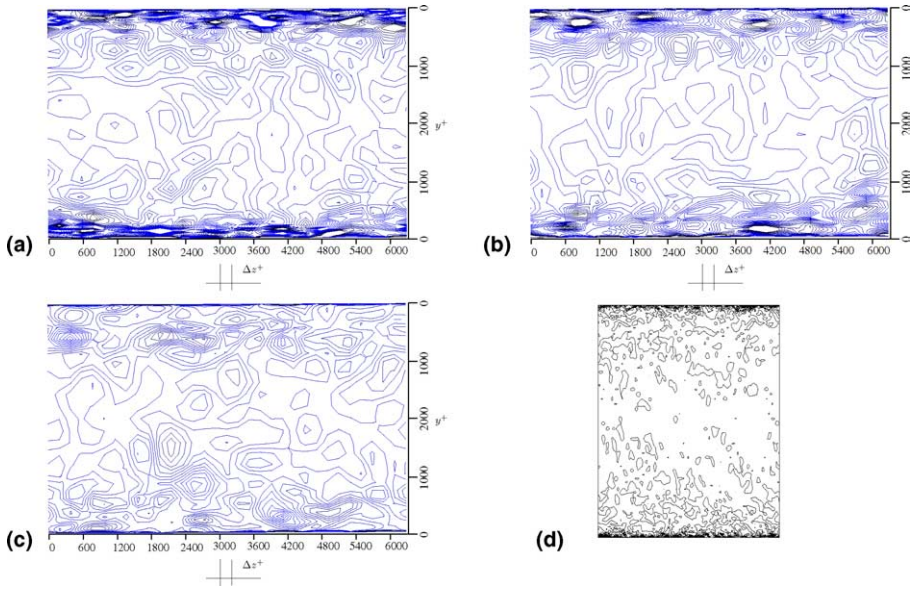

Fig. 15. Contours of streamwise vorticity in planes normal to the flow: (a) $y^+_{int} = 120$, with $C^{av}_{\mu,int}$; (b) $y^+_{int} = 280$, with $C^{inst}_{\mu,int}$; (c) $y^+_{int} = 610$, with $C^{inst}_{\mu,int}$. (d) Fine-grid (reference) LES.

distance to neighbours remains roughly the same, this distance being determined by the mesh spacing in the spanwise direction. However, in Fig. 15b, the interface is already at the edge of streaks-populated region, and in Fig. 15c, much beyond it.

The seemingly paradoxical finding that better predictions of velocity and second-moment turbulence statistics are obtained when the RANS/LES interface is placed further from wall, thus leading to a loss of the near-wall turbulence structure, is disconcerting on fundamental grounds. However, viewed pragmatically, this has favourable implications in respect of simulating complex flows at very high Reynolds numbers. In such cases, a substantial portion of the thin boundary layers cannot be resolved in any event, and the interface must inevitably be placed at high y^+ values.

4. Results for separated flow

In this section, the hybrid RANS/LES approach is applied to the case of a separated flow in a channel, one wall of which forms hill-shaped periodic constrictions which are spaced at intervals of nine hill heights. The computational domain consists of one periodic segment. The Reynolds number, based on bulk velocity and the total channel height, is 21,560. This value is considerably lower than is desirable. However, the evaluation of the hybrid method relies critically on the availability of highly-resolved LES data, and such data are extremely rare for high-Reynolds-number separated flow. The data used here arise from a carefully undertaken (and costly) simulation on a 4.7-million-node mesh (Temmerman et al., 2003).

Figs. 16 and 21, to be discussed later in detail, convey an overall view of the flow. The flow separates slightly downstream of the hill crest and reattaches at about half of the inter-hill span. Following reattachment, the flow recovers for some distance before being accelerated over the next hill.

The simulations discussed herein are summarised in Table 1. In total, four simulations were performed using the hybrid approach that combines the Wolfshtein one-equation model in the RANS layer with the

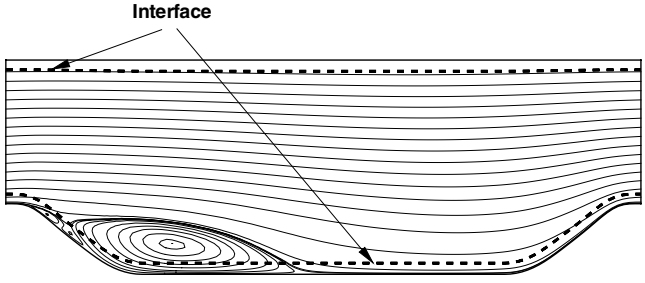

Fig. 16. Streamlines for an hybrid RANS/LES simulation with $C_\mu = 0.09$ and the interface located at $j = 13$.

Table 1
Description of the grids and locations of separation and reattachment

Case	Cells number	$(x/h)_{sep.}$	$(x/h)_{reat.}$	Interface location (j)
Ref.	$196 \times 128 \times 186$	0.22	4.72	–
LES	$112 \times 64 \times 56$	0.23	4.64	–
HRL-j5	$112 \times 64 \times 56$	0.25	5.43	5
HRL-j9	$112 \times 64 \times 56$	0.23	5.65	9
HRL-j13	$112 \times 64 \times 56$	0.23	5.76	13
HRL-j18	$112 \times 64 \times 56$	0.23	5.69	18

one-equation SGS model of Yoshizawa and Horiuti (1985) in the LES region. The grid used for all cases reported contains $112 \times 64 \times 56 = 4 \cdot 10^5$ cells, compares with $196 \times 128 \times 186 = 4.7 \cdot 10^6$ cells for the highly-resolving reference-LES mesh. In both grids, the centroids of the near-wall cells are located below $y^+ = 1$ over most of the flow domain.

A first, preliminary, computation (not listed in Table 1) was performed *without* the dynamic adjustment of the C_μ coefficient; that is, C_μ was maintained at 0.09 throughout the RANS region. The outcome is conveyed only by the time-averaged streamfunction field shown in Fig. 16. In this, the dashed wall-parallel lines identify the locations of the interface between the RANS and LES regions. The resulting flow features two small recirculation zones upstream of a third largest one, and this is not in accord with the reference solution, Fig. 21. Moreover, reattachment is premature and the recirculation zone is too small.

The remaining four HRL computations used the adaptive procedure as described in Section 3. The difference among the four computations lies in the location of the interface, indicated by the number of grid cells included in the RANS layer in the right-most column of Table 1). Fig. 17 shows the location of the lower-wall interface relative to the wall, expressed in wall units. As seen, the interface-to-wall distance reaches $y^+ =$ 100–200 over a significant proportion of the domain. In agreement with observations derived from channel-flow simulations, the interface value determined from the dynamic process varies substantially with the interface position. This is demonstrated in Fig. 18. The further away the interface is from the wall, the lower the value of the interface C_μ coefficient. In the present flow, there are obviously substantial streamwise variations along the interface, and these changes are reflected by correspondingly substantial streamwise variations in the coefficient. Fig. 19 shows cross-RANS-layer distributions of C_μ at three streamwise locations, all derived from the appropriate interface value and Eq. (9). As

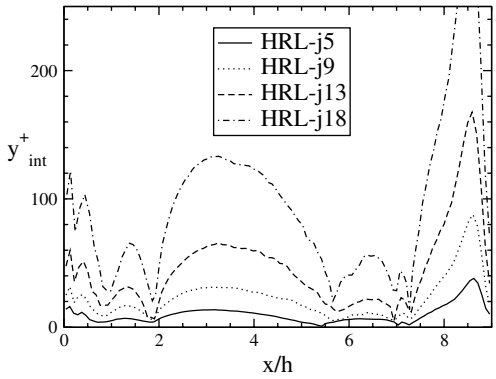

Fig. 17. Location of the lower interface for all four cases considered (expressed in wall units).

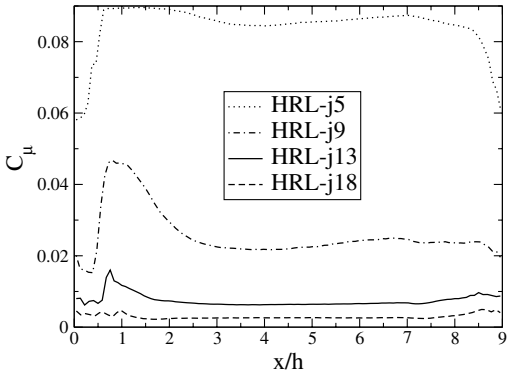

Fig. 18. Averaged $C_{\mu,\mathrm{int}}$ distribution along the lower interface for all four cases.

was observed in the channel-flow simulations, the distributions are, here too, bunched together, and this may be taken to indicate that the assumed shape of C_μ imposed by Eq. (9) gives a realistic variation within the RANS layer, even when the interface is far from the wall. An exception arises in the simulation HRL-j5. In this case, the interface is very close to the wall, and C_μ at the interface is computed to be close to 0.09, thus suggesting that

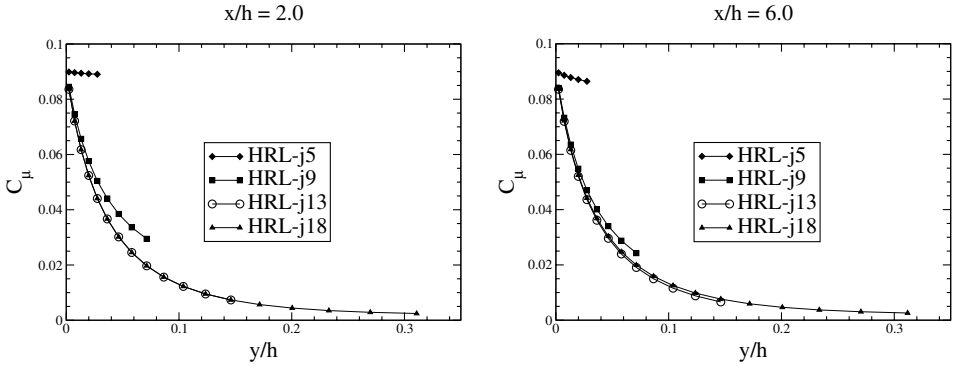

Fig. 19. Averaged $C_{\mu,\mathrm{int}}$ distribution in the vertical direction in the lower near-wall region for all four cases.

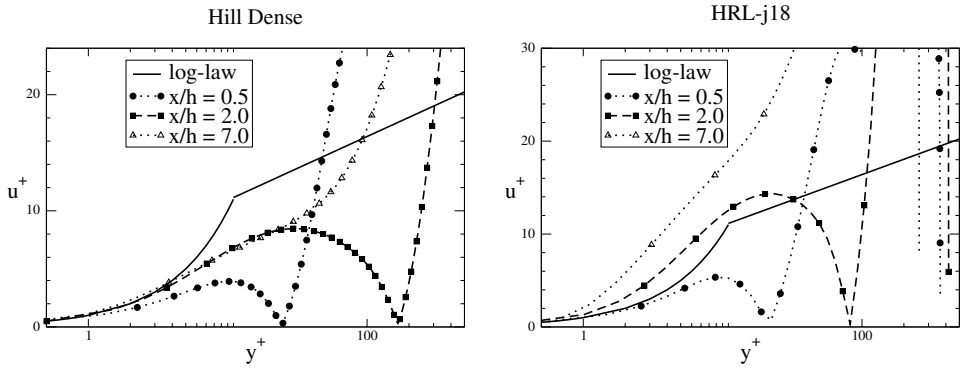

Fig. 20. Velocity profiles expressed in wall units for the lower wall region, for the reference case and the case $j = 18$.

the assumed C_μ distribution is not correct very close to the wall. However, as the contribution of the RANS model in this region is insignificant, this erroneous behaviour is unlikely to be of major consequence. The similarity in the present behaviour of C_μ to that for the plane channel flow is remarkable when contrasted with the drastic differences in the structure of the near-wall region in these two flows. These differences are conveyed in Fig. 20 which compares wall-scaled velocity profiles from the highly-resolved LES and the HRL-j18 solution at three streamwise locations. Both sets of profiles demonstrate that the near-wall flow is here far from the log-law which characterises the plane channel flow. While the hybrid solution does evidently not return profiles which agree well with the highly resolved LES, if only because the recirculation zones differ in size, corresponding distributions clearly show qualitatively similar features.

Table 1 includes the time-mean separation and reattachment locations for the various simulations. For all four cases, the location of the separation point is well predicted. However, reattachment occurs 0.7–1.1 hill heights downstream of that given by the reference simulation. In contrast, the reattachment location predicted by the pure LES solution on the HRL grid, while a little short, is close to the reference value. Prima facie, this outcome is disappointing, but not entirely surprising, for the HRL grid provides, at the relatively low Reynolds number of the present flow, a reasonable resolution of the near-wall region. However, an encouraging message is that the RANS region can be varied over a substantial range of wall-layer thickness without detrimental consequences to the solution. The fact that all HRL simulation give similar reattachment locations is significant, and suggests an underlying deficiency in the RANS representation. Indeed, tests have shown that the imposition of the correct wall-shear stress distribution onto the HRL simulations, in place of that actually predicted by the HRL simulation, drastically improved the reattachment location. This, as well as further tests not detailed herein, provide credible evidence that the

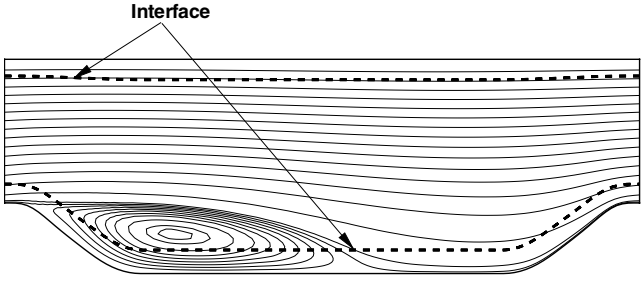

Fig. 21. Streamlines for an hybrid RANS/LES simulation with the interface located at $j = 18$.

excessive reattachment length predicted by all HRL simulations is due to the RANS model (a one-equation formulation!) returning inaccurate wall shear stress values, especially in the vicinity of the reattachment point. Further results presented below relate mainly to the case $j = 18$, the thickest RANS layer, as all other simulations yielded similar flow characteristics.

Fig. 21 gives the streamfunction field for simulation HRL-j18. The dashed lines indicate the interface locations, and it is noted that the lower-wall RANS layer extends almost to the centre of the recirculation zone. The two small bubbles observed in Fig. 16 no longer appear. As noted already, however, the recirculation zone is considerably longer than the reference value, and this is the major reason for the differences in the velocity profiles shown in Fig. 22.

Notwithstanding the relatively low Reynolds number, Fig. 24 shows that the turbulent viscosity in the near-wall layers is substantially elevated when the RANS layers are thick, as is the case with HRL-j18 for which y^+ is of the order 100–200. Hence, the hybrid RANS–LES scheme is clearly effective in so far as it causes a significant increase in the proportion of the near-wall turbulence activity carried by the RANS model. The oscillatory features observed around the interface reflect slight corresponding oscillations in the turbulence energy, caused by the combination of flow complexity within the thick layers, the explicit solution

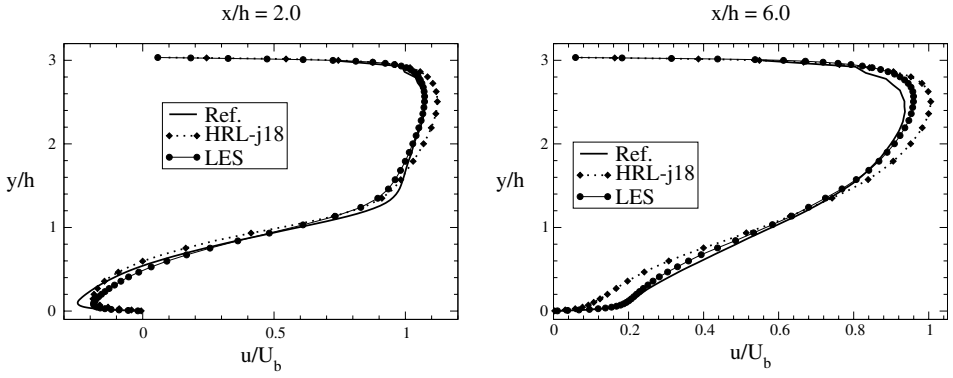

Fig. 22. Streamwise velocity profiles at three different streamwise locations.

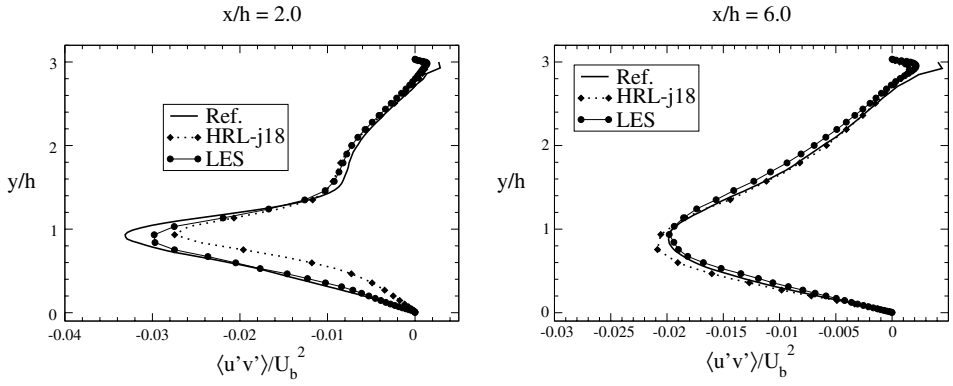

Fig. 23. Resolved shear stress at three different streamwise locations.

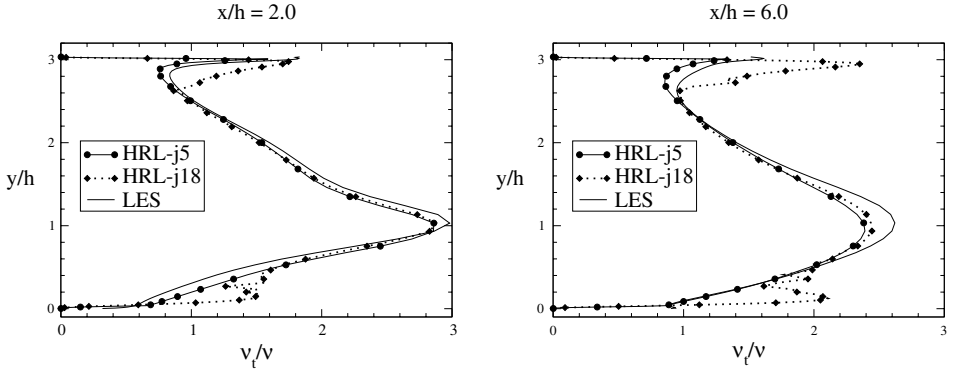

Fig. 24. Modelled viscosity at three different streamwise locations for the cases $j = 5$ and $j = 18$ and for a LES with the Yoshizawa and Horiuti model.

of the turbulence energy and the use of central differences for turbulence convection. Despite the major alteration of the turbulence characteristics in the near-wall layer caused by the RANS model, the simulation has not suffered, except for the elongation of the recirculation zone, which has already been argued to be a response to defects in the wall-shear stress. In particular, the total shear stress is well reproduced, as shown in Fig. 23.

5. Concluding remarks

Based on our exploration and related work reported in the literature, it is justified to conclude that hybrid RANS/LES models of the type introduced herein are feasible and promising. Most hybrid models give substantially better solutions than the equivalent coarse-grid LES. It is likely, therefore, that they will increasingly be used for the simulation of complex flows

at high Reynolds numbers. Extensive testing over the past few years of a substantial number of alternative formulations has demonstrated that, notwithstanding the significant advantages derived from hybrid modelling, no model form yields an entirely satisfactory representation of near-wall turbulence with a RANS-type grid. The main source of defects is that, irrespective of the model used, insufficient near-wall grid resolution simply cannot capture the details of the small-scale streaky structure near the wall. However, the imperfection of hybrid models needs to be viewed against the fact that these use, at elevated Reynolds numbers, a small fraction of the number of cells required for trustworthy, well-resolved LES: for the channel flow discussed in this paper, the hybrid grid had less than 1% of cells of the fine LES grid.

The zonal approach seems especially appealing, because outside the wall boundary layers, the conventional LES method is used without any intervention in respect of sub-grid-scale modelling. However, even if the RANS model is adjusted to meet the constraints of continuity of eddy viscosity, as well as other quantities at the interface, an insufficient level in small-scale activity that the RANS feeds into the LES across the interface produces, in most circumstances, non-physical features in the velocity profile around the interface. Another problem in zonal modelling is the need to prescribe the interface location, although this can be automated, in principle, in terms of grid spacing. As regards the sensitivity of the solution to the interface location, the present study has shown that placing the RANS/LES interface close to the wall ($y^+ \leqslant 120$) produces too low levels of eddy viscosity. Beyond a distance $y^+ = 280$, the position of the interface becomes less influential. The mean-velocity profile is influenced predominantly by the modelled viscosity up to $y^+ = 120$. The anomalous kink observed in the velocity profile in the interface region appears to be caused by the rapid change in viscosity across the interface, rather than by inappropriate local interface properties.

It has been observed that most of the hybrid models, including DES, reproduce better the log-law when the interface is moved away from the wall. This appears paradoxical in view of the fact that the use of the RANS strategy over a larger region diminishes the realism with which structural features are captured. The interface anomaly diminishes also when the interface is moved *very* close to the wall, say around or below $y^+ = 30$, but this requires an increasingly high grid density, negating the main goal of the hybrid approach.

The application of the method to a single recirculating flow is somewhat inconclusive, primarily because of the low Reynolds number of the flow. This constrained the choice of an appropriately coarse grid which would challenge the method and would be expected to yield poor results for pure LES computations on that grid. For this flow, the LES/RANS method results in an excessively long recirculation zone. There is firm evidence to suggest, however, that this stems from defects in the wall-shear stress returned by the RANS model, rather than from a fundamental limitation of the hybrid formulation. A decidedly encouraging observation is that the solutions are only weakly sensitive to the location of the interface, even if this extends deep into the flow, and in near-wall conditions far removed from those corresponding to turbulence equilibrium.

Acknowledgements

The authors are grateful to the UK Engineering and Physical Sciences Research Council (EPSRC) for providing financial support for the research reported herein. This included an EPSRC Visiting Fellowship, enabling Prof. K. Hanjalić to spend three months at Imperial College London. Computer resources, also awarded by EPSRC, as part of the work programme of the HPC Consortium LESUK-2, were provided by the CSAR National Centre at the University of Manchester.

References

Abe, K., Kondoh, T., Nagano, Y., 1994. A new turbulence model for predicting fluid flow and heat transfer in separating and reattaching flows—I. Flow field calculations. Int. Journal of Heat and Mass Transfer 37, 139–151.

Balaras, E., Benocci, C., 1994. Subgrid-scale models in finite-difference simulations of complex wall bounded flows. In: 74th Fluid Dynamic Symp. on Applications of Direct and Large Eddy Simulation, pp. 2-1–2-6.

Balaras, E., Benocci, C., Piomelli, U., 1996. Two-layer approximate boundary conditions for large-eddy simulations. AIAA J. 34, 1111–1119.

Cabot, W., Moin, P., 1999. Approximate wall boundary conditions in the large eddy simulation of high Reynolds number flow. Flow, Turbulence and Combustion 63, 269–291.

Chapman, D., 1979. Computational aerodynamics, development and outlook. AIAA J. 17, 1293–1313.

Davidson, L., Peng, S.-H., 2001. A hybrid RANS–LES model based on a one-equation SGS model and a two-equations k–ω model. In: Lindborg, E., et al (Eds.), Proc. 2nd Symp. on Turbulence and Shear Flow Phenomena, pp. 175–180.

Deardorff, J., 1970. A numerical study of three-dimensional turbulent channel flow at large Reynolds number. J. Fl. Mech. 61, 481–507.

Diurno, G., Balaras, E., Piomelli, U., 2001. Wall-layer models for LES of separated flows. In: Geurts, B. (Ed.), Modern simulation strategies for turbulent flows, pp. 207–222.

Hanjalić, K., Hadžiabdić, M., Temmerman, L., Leschziner, M., 2004. Merging LES and RANS strategies: zonal or seamless coupling. In: Friedrich, R., Geurts, B., Métais, O. (Eds.), Direct and Large-Eddy Simulations V. Kluwer Academic Publishers, pp. 451–464.

Hoffman, G., Benocci, C., 1995. Approximate wall-boundary conditions for large-eddy simulations. In: Benzi, R. (Ed.), Advances in Turbulence V. Kluwer Academic Publishers, pp. 222–228.

Nicoud, F., Ducros, F., 1999. Subgrid-scale stress modelling based on the square of the velocity gradient tensor. Flow, Turbulence and Combustion 62, 183–200.

Norris, L., Reynolds, W., 1975. Turbulence channel flow with a moving wavy boundary. Technical reports, Department of Mechanical Engineering, Stanford University.

Piomelli, U., Balaras, E., Pasinato, H., Squires, K., Spalart, P., 2003. The inner-outer layer interface in large-eddy simulations with wall-layer models. Int. J. Heat and Fluid Flow 24, 538–550.

Schumann, U., 1975. Subgrid scale models for finite difference simulations of turbulent flows in plane channels and annuli. J. Comp. Phys. 18, 376–404.

Shur, M., Spalart, P., Strelets, M., Travin, A., 1999. Detached-eddy simulation of an airfoil at high angle of attack. In: Rodi, W., Laurence, D. (Eds.), Engineering Turbulence Modelling and Experiments-4. Elsevier Science, pp. 669–678.

Smagorinsky, J., 1963. General circulation experiments with the primitive equations, I, the basic experiment. Mon. Weather Rev. 91, 99–165.

Spalart, P., Allmaras, S., 1992. A one-equation turbulence model for aerodynamic flows. In: AIAA Paper 92-0439.

Spalart, P., Jou, W.-H., Strelets, M., Allmaras, S., 1997. Comments on the feasibility of LES for wings and on the hybrid RANS/LES approach. In: Advances in DNS/LES, 1st AFOSR Int. Conf. on DNS/LES. Greden Press.

Temmerman, L., Leschziner, M., Mellen, C., Fröhlich, J., 2003. Investigation of subgrid-scale models and wall-function approximations in Large Eddy Simulation of separated flow in a channel with streamwise periodic cosntrictions. Int. J. Heat and Fluid Flow 24, 157–180.

Temmerman, L., Leschziner, M., Hanjalić, K., 2003. A combined RANS–LES strategy with arbitrary interface location for near-wall flows. In: Kasagi, N., et al. (Eds.), Proc. 3rd Symp. on Turbulence and Shear Flow Phenomena, 929–934.

Wang, M., Moin, P., 2000. Computation of trailing edge flow and noise using large-eddy simulation. AIAA J. 38 (12), 2201–2209.

Wei, T., Willmarth, W., 1998. A selection of test cases for the validation of large-eddy simulations of turbulent flows. Vol. AGARD-AR-345. AGARD, p. 122.

Werner, H., Wengle, H., 1991. Large eddy simulation of turbulent flow over and around a cube in a plate channel. In: 8th Symp. on Turb. Shear Flows, pp. 155–168.

Wolfshtein, M., 1969. The velocity and temperature distribution in one dimensional flow with turbulence augmentation and pressure gradient. Int. J. Heat Mass Transfer 12, 301–318.

Yoshizawa, A., Horiuti, K., 1985. A statistically-derived subgrid-scale kinetic energy model for the large-eddy simulation of turbulent flows. J. Phys. Soc. Jpn. 54, 2834–2839.